Determination of tilt degree and Weyl-node separation by the spatial Imbert-Fedorov shift near the Brewster angle

Jipeng Wu,[1,2] Leyong Jiang,[3] Rongzhou Zeng,[2] Jiaojiao Liang,[2] Xiaoyu Dai,[1] and Yuanjiang Xiang[1,*]

[1]*School of Physics and Electronics, Hunan University, Changsha 410082, China*

[2]*College of Railway Transportation, Hunan University of Technology, Zhuzhou 412007, China*

[3]*School of Physics and Electronics, Hunan Normal University, Changsha 410081, China*

(Received 7 September 2021; accepted 26 January 2022; published 11 February 2022)

The Imbert-Fedorov (IF) shift at the optical interface of Weyl semimetal (WSM) is extremely significant to recognize the optical characteristics of WSM. In this paper, we have studied the spatial IF shift on the surface of a bulk WSM by theoretically deriving a 4×4 magneto-optic matrix. It is found that the phenomenon of spatial IF shift changing from positive to negative occurs at an incident angle near the Brewster angle. Remarkably, this special phenomenon can be regulated by changing the frequency of incident light, tilt degree, and Weyl node separation. Specially, for a fixed Weyl node separation, the phenomena of spatial IF shift changing from positive to negative can be realized at different tilt degrees by simply changing the frequency, and there exists one-to-one correspondence between the tilt degree and frequency at these situations. Similarly, for a fixed tilt degree, these phenomena can be achieved at different Weyl node separations by changing the frequency, and there also exists one-to-one correspondence between the Weyl node separation and frequency. Therefore, these tunable phenomena of spatial IF shift changing from positive to negative enable the feasibility of accurate determination of tilt degree and Weyl node separation. Our study can also provide a reference for the research of IF shift in such similar structures.

DOI: 10.1103/PhysRevA.105.023508

I. INTRODUCTION

A Weyl semimetal (WSM), as a remarkable topological quantum state with nonmass Weyl fermions as quasiparticles, occurs only when the symmetry of spatial inversion or time inversion is broken [1–3]. Similar to the famous semimetal graphene, WSM shows a Dirac-like linear dispersion, thus is called "three-dimensional graphene." Because of its Dirac-like linear dispersion, WSM exhibits many outstanding optical characteristics, such as unique optical nonlinearity [4–6] and adjustable terahertz plasmon resonance [7]. Differently, compared with the two-dimensional Hamiltonian of grapheme, WSM has the three-dimensional Hamiltonian, which results in many special physical properties, such as chiral anomalies [8], epsilon-near-zero response [9], unconventional quantum Hall effect [10], etc. Notably, with the discovery of Fermi arc and Weyl points (WPs) [11–14], it is easy to distinguish WSM from graphene. Generally, since the Weyl cones near the WPs exhibit upright, the Weyl fermions satisfy the Lorentz symmetry, and the WSM materials, such as TaAs family, are defined as type-I WSMs [15]. However, if the Weyl cones exhibit heavily tilted, exceeding the Fermi velocity, the Weyl fermions do not satisfy the Lorentz symmetry, and the WSM materials, such as WTe_2 and $MoTe_2$, are defined as type-II WSMs [16–18]. In order to distinguish type-I and type-II WSMs, a tilt degree α_t of Weyl cones is introduced (the tilt degree of Weyl cones is $|\alpha_t| < 1$ in type-I WSMs, while it is $|\alpha_t| > 1$ in type-II WSMs). Additionally, the Weyl nodes in a WSM serve as a source or sink of the Berry curvature, acting as a magnetic field in the momentum space [19–22], resulting in that the optical responses in WSMs need to be described by means of the modified Maxwell equations, known as axion electrodynamics [23,24]. Similarly, the separation between WPs in the z direction in momentum space is defined by $2Q$, where Q denotes the Weyl node separation [25]. Unlike Dirac materials such as graphene, the tilt degree and Weyl node separation are two unique and extremely important parameters for determining the optical properties of WSM. Methods for effectively obtaining these two parameters have therefore achieved great significance for us to recognize the optical characteristics of WSM.

The Imbert-Fedorov (IF) shift, as one of the most extensive optical effects of beam reflecting at the interface of medium, presents as the spin-dependent splitting caused by transverse separation of photons with opposite spin angular momentums [26–28]. The IF shift exhibits sensitivity to the configuration parameters of materials, resulting in that the precision metrology can be realized by using the IF shift as a probe. For instance, the thickness of metal film and the layers of graphene were successfully obtained by means of IF shift [29,30], and the detection of DNA hybridization was fulfilled with the help of a highly sensitive optical biosensor [31]. Recently, with the research hotspots of WSM, the IF shift based on WSM has also been widely studied. Jiang *et al.* proposed that the IF shift existed and exhibited susceptibility to the valley in a WSM system, and demonstrated that the IF shift provided an effective method to determine electrical

*xiangyuanjiang@126.com

conductivity of WSM [32,33]. Chen *et al.* investigated the IF shift on the interface of a WSM film, and further discussed the relationship between the Weyl node separation of WSM and the spin-dependent splitting [34]. Liu *et al.* demonstrated that the IF shift in a WSM was affected by the lattice spacing, and proposed a simple method to sense the lattice spacing precisely [35]. Nevertheless, most of these studies focus on the realization and the influence of IF shift in WSM based systems. Precision metrology acts as an important aspect of application of IF shifts, but there exist few reports on the measurement of WSM. Therefore, it is of great significance for us to realize the measurement of the relevant parameters of WSM, such as the tilt degree and Weyl node separation.

In this article, we theoretically study the spatial IF shift at the contact surface of air and bulk WSM. We set up a 4×4 magneto-optic matrix by using Maxwell's equations and boundary conditions to obtain the calculation of spatial IF shift. Results show that the spatial IF shift changes its sign from positive to negative in a small region of incident angle of 50°. It is further demonstrated that this special phenomenon is caused by Brewster effect. Remarkably, this special phenomenon can be regulated by changing the frequency of incident light, tilt degree, and Weyl node separation. Specially, for a fixed Weyl node separation, the phenomena of spatial IF shift changing from positive to negative can be realized at different tilt degrees by simply changing the frequency, and there exists one-to-one correspondence between the tilt degree and frequency at these situations. Therefore, we can accurately obtain the tilt degree based on these special phenomena by shifting the frequency. Similarly, for a fixed tilt degree, the tunable phenomena of spatial IF shift changing from positive to negative with one-to-one correspondence between the Weyl node separation and frequency enable the feasibility of accurate calculation of Weyl node separation. We believe our study may provide a reference to research the IF shift in such similar structures.

II. THEORETICAL MODEL AND METHOD

We theoretically set up a simple model to investigate the IF shift on the surface of a bulk WSM, as shown in Fig. 1(a). The thickness of bulk WSM is optimized to be $d = 600$ nm, which is exposed in air. Considering a line polarized light illuminating the surface of bulk WSM with incident angle θ, the right- and left-spin lights separate from each other in reflected light, resulting in the phenomenon of IF shift. Figures 1(b) and 1(c) represent the type-I ($|\alpha_t| < 1$) and type-II ($|\alpha_t| > 1$) WSMs, respectively, in which Q denotes the Weyl node separation.

A. Optical constant of WSM

For WSMs with time-reversal symmetry broken, we consider them as a simple continuum model that a wave vector $\pm b = \pm(0, 0, Q)$ in the Brillouin zone separates a pair of Weyl points (WPs) with opposite chirality $\xi = \pm 1$. Here, Q denotes the Weyl node separation (in the z direction). Near the two WPs located at $Q\vec{z}$, the Hamiltonian of the WSMs can be described as [25]

$$\hat{H}_0 = \sum_k h_k \cdot \sigma, \tag{1}$$

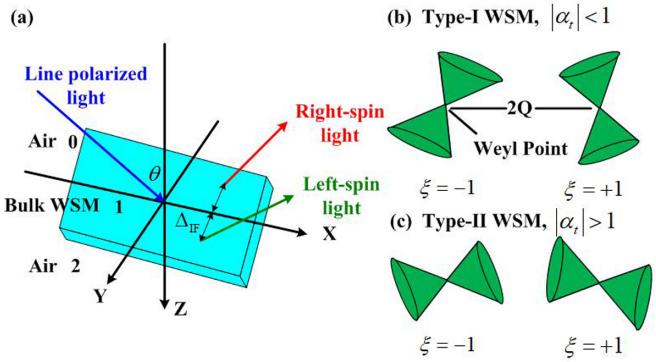

FIG. 1. Schematic exhibiting the IF shift on the surface of a bulk WSM with tilt degree and Weyl node separation. (a) A line polarized light illuminates a bulk WSM which is exposed in air, and the IF shift occurs in reflected light for the separation of right- and left-spin lights. (b) A pair of tilted Weyl cones with opposite chirality in type-I WSM with a tilt degree $|\alpha_t| < 1$, in which Q represents the Weyl node separation. (c) A pair of tilted Weyl cones with opposite chirality in type-II WSM with a tilt degree $|\alpha_t| > 1$.

where $h_k = (h_{ok}, h_{1k}, h_{2k}, h_{3k})$ represents the vector which is the function of scalar k; $h_{ok} = \hbar\xi v_t k_z^\xi$, $h_{1k} = \hbar\xi v_F k_x$, $h_{2k} = \hbar\xi v_F k_y$, and $h_{3k} = \hbar\xi v_F k_z^\xi$; σ is the vector composed of the identity and the three 2×2 Pauli matrices σ_x, σ_y, and σ_z. Therefore, we can obtain the low-energy Hamiltonian of the WPs with chirality ξ, described as

$$\vec{H}_\xi = \hbar\xi v_t k_z^\xi + \xi\hbar v_F\left[k_x\sigma_x + k_y\sigma_y + k_z^\xi\sigma_z\right], \tag{2}$$

with $k_z^\xi = k_z + \xi Q$. The Weyl cones near the two WPs are oppositely tilted, and the Weyl cone can be described by the parameter of tilt degree $\alpha_t = v_t/v_F$. Where v_t and v_F represent the tilt velocity of WPs with positive chirality and the Fermi velocity, respectively. For type-I WSMs, the tilt degree meets $|\alpha_t| < 1$, while $|\alpha_t| > 1$ for type-II WSMs [15,16]. In order to simplify the discussion, we mainly discuss the case of $\alpha_t > 0$, and the case of $\alpha_t < 0$ can be similarly handled.

For a bulk WSM, we can use a 3×3 tensor to describe its conductivity, written as

$$\overline{\overline{\sigma}} = \begin{pmatrix} \sigma_{xx} & \sigma_{xy} & 0 \\ \sigma_{yx} & \sigma_{yy} & 0 \\ 0 & 0 & \sigma_{zz} \end{pmatrix}, \tag{3}$$

where σ_{xy} and σ_{yx} correspond to the Hall conductivities with $\sigma_{xy} = -\sigma_{yx}$, and σ_{xx} and σ_{yy} denote the longitudinal conductivities with $\sigma_{xx} = \sigma_{yy}$, and the corresponding expressions of conductivity are detailed in the Appendix.

By calculating the conductivities of WSM, its relative dielectric constant is readily expressed in terms of the optical conductivities and the internode separation, described as [25]

$$\begin{aligned} \varepsilon_{xx} &= \varepsilon_b + \frac{i\sigma_{xx}}{\omega\varepsilon_0}, \\ \varepsilon_{zz} &= \varepsilon_b + \frac{i\sigma_{zz}}{\omega\varepsilon_0}, \\ \varepsilon_{xy} &= \frac{i}{\omega\varepsilon_0}(\sigma_{xy} + \sigma_Q), \end{aligned} \tag{4}$$

where ε_0 is the permittivity of vacuum; ε_b denotes the effective permittivity of the background medium, which is set as $\varepsilon_b = 1$ in this article.

B. 4 × 4 magneto-optical matrix

Considering an electromagnetic wave illuminating our designed structure from air shown in Fig. 1, reflection occurs at the contact surface of air and bulk WSM. In our designed structure, for a pair of nodes separated along the k_z direction in the bulk BZ, the x-y plane has no Fermi arc states. The incident light illuminates the surface of bulk WSM (x-y plane), there is no surface conductivity at the $z = 0$ and $z = d$ boundary since the projection of the vector is zero in this case, thus the tangential electric and magnetic fields keep continuous at the $z = 0$ and $z = d$ surface [36–38]. Therefore, the Fermi arc does not affect the reflection coefficient significantly. Due to the polarization separation of electromagnetic waves in a WSM [36,39], the traditional transfer matrix method is unsuitable for solving the reflection coefficients, and we introduce a 4×4 magneto-optical matrix to solve the problem.

First, the dispersion equation of the wave vector in a WSM is studied by using Maxwell's equations. In regions 0, 1, and 2, the Maxwell equations can be written as

$$\nabla \times \vec{E}_i = i\omega\mu_0 \vec{H}_i, \tag{5a}$$

$$\nabla \times \vec{H}_i = -i\omega \vec{D}_i, \tag{5b}$$

where $i = 0, 1, 2$. Within the WSM, $i = 1$, by using the wave vector $\vec{k}_1$ to replace the spatial derivatives, Eqs. (5a) and (5b) can be expressed as $\vec{k}_1 \times \vec{E}_1 = \omega\mu_0 \vec{H}_1$ and $\vec{k}_1 \times \vec{H}_1 = -\omega\varepsilon_0 \bar{\bar{\varepsilon}} \vec{E}_1$, in which $\bar{\bar{\varepsilon}}$ denotes the tensor of the WSM. Simultaneously, we use $\vec{k}_1$ to cross the first equation above, and combine the second equation; thus the relationship between $\vec{k}_1$ and $\vec{E}_1$ is expressed as

$$\vec{k}_1 \times (\vec{k}_1 \times \vec{E}_1) = -k_0^2 \bar{\bar{\varepsilon}} \vec{E}_1. \tag{6}$$

By using $\vec{k}_1 = k_{1x}\vec{x} + k_{1z}\vec{z}$, Eq. (6) can be written as a matrix expression,

$$\begin{pmatrix} k_0^2\varepsilon_{xx} - k_{1z}^2 & ik_0^2\gamma & k_{1z}k_{0x} \\ ik_0^2\gamma & k_\perp^2 - k_0^2\varepsilon_{xx} & 0 \\ k_{1z}k_{0x} & 0 & k_0^2\varepsilon_{zz} - k_{0x}^2 \end{pmatrix} \begin{pmatrix} E_{x1} \\ E_{y1} \\ E_{z1} \end{pmatrix} = 0, \tag{7}$$

where $k_\perp = \sqrt{k_{1z}^2 + k_{1x}^2}$, $\gamma = \varepsilon_{xy}/i$, $k_0 = \omega/c$, $k_{0x} = k_0 \sin\theta$. Because of translational invariance, the transverse component of the wave vector is equal in each layer, $k_{1x} = k_{2x} = k_{0x}$. Due to the polarization separation of light propagating in the WSM, there exist three electric field components. The condition for the existence of a nonzero solution to the electric field in Eq. (7) is that the modulus of the coefficient matrix is zero, so we can get the solution of k_{1z}, denoted by k_+ and k_- as

$$k_\pm^2 = \frac{k_0^2}{2\varepsilon_{zz}}\Big[2\varepsilon_{xx}\varepsilon_{zz} - (\varepsilon_{xx} + \varepsilon_{zz})\sin^2\theta \pm \sqrt{(\varepsilon_{zz} - \varepsilon_{xx})^2\sin^4\theta - 4\varepsilon_{zz}\gamma^2\sin^2\theta + 4\varepsilon_{zz}^2\gamma^2}\Big]. \tag{8}$$

In order to obtain the spatial IF shift at the contact surface of air and bulk WSMs, the relevant reflection coefficients r_{pp}, r_{sp}, r_{ss}, and r_{ps} should be calculated, which are defined as $r_{pp} = E_r^p/E_i^p$, $r_{sp} = E_r^p/E_i^s$, $r_{ss} = E_r^s/E_i^s$, and $r_{ps} = E_r^s/E_i^p$, where E_i^p and E_i^s denote the amplitude of electric field of incident light for a TM- and TE-polarized wave, and E_r^p and E_r^s exhibit the amplitude of electric field of reflected light for a TM- and TE-polarized wave.

For a TM-polarized wave, the incident magnetic field thus can be described as $\vec{H}_i = H_{y00}\vec{y}e^{i(k_{0x}x + k_{0z}z)}$. By using the Maxwell equation $\nabla \times \vec{H} = -i\omega\vec{D}$, the corresponding incident electric field can be simply obtained as $\vec{E}_i = Z_0(\cos\theta\vec{x} - \sin\theta\vec{z})e^{i(k_{0x}x + k_{0z}z)}$, in which Z_0 denotes the wave impedance in vacuum, and the amplitude of electric field is in units of H_{y00}. The incident light reflects at the contact surface of air and bulk WSM, resulting in the magnetic field in region 0 written in terms of incident and reflected waves, shown as

$$H_{x0} = r_3 e^{-ik_{0z}z}e^{ik_{0x}x}, \quad H_{y0} = (e^{ik_{0z}z} + r_1 e^{-ik_{0z}z})e^{ik_{0x}x}, \quad H_{z0} = r_2 e^{-ik_{0z}z}e^{ik_{0x}x}. \tag{9}$$

By using the Maxwell's equation $\nabla \cdot \vec{H}_0 = 0$, we get the relationship $r_3 = k_{0z}r_2/k_{0x}$. Meanwhile, by using $\nabla \times \vec{H} = -i\omega\vec{D}$, the electric field in region 0 is written as

$$E_{x0} = Z_0\frac{k_{0z}}{k_0}(e^{ik_{0z}z} - r_1 e^{-ik_{0z}z})e^{ik_{0x}x}, \tag{10a}$$

$$E_{y0} = Z_0\frac{k_0}{k_{0x}}r_2 e^{-ik_{0z}z}e^{ik_{0x}x}, \tag{10b}$$

$$E_{z0} = -Z_0\frac{k_{0x}}{k_0}(e^{ik_{0z}z} + r_1 e^{-ik_{0z}z})e^{ik_{0x}x}. \tag{10c}$$

For region 1, the general solution of the electric field is described as linear combination of the four wave-vector components, $k_{1z} = \{k_+ \quad -k_+ \quad k_- \quad -k_-\}$:

$$E_{1y} = (a_1 e^{ik_+z} + a_2 e^{-ik_+z} + a_3 e^{ik_-z} + a_4 e^{-ik_-z})e^{ik_{0x}x}; \tag{11}$$

by using Eqs. (5a) and (5b), the other components of electric and magnetic fields can be obtained as >

$$E_{1x} = \frac{i}{\gamma k_0^2}\Big[\big(k_+^2 + k_{0x}^2 - \varepsilon_{//}k_0^2\big)(a_1 e^{ik_+z} + a_2 e^{-ik_+z}) + \big(k_-^2 + k_{0x}^2 - \varepsilon_{//}k_0^2\big)(a_3 e^{ik_-z} + a_4 e^{-ik_-z})\Big]e^{ik_{0x}x}, \tag{12a}$$

$$E_{1z} = \frac{ik_{0x}}{\gamma k_0^2\big(k_{0x}^2 - \varepsilon_{zz}k_0^2\big)}\Big[\big(k_+^2 + k_{0x}^2 - \varepsilon_{//}k_0^2\big)k_+ \times (a_1 e^{ik_+z} - a_2 e^{-ik_+z}) + \big(k_-^2 + k_{0x}^2 - \varepsilon_{//}k_0^2\big) \times k_-(a_3 e^{ik_-z} - a_4 e^{-ik_-z})\Big]e^{ik_{0x}x}, \tag{12b}$$

$$H_{1x} = -\frac{1}{Z_0 k_0}(k_+ a_1 e^{ik_+z} - k_+ a_2 e^{-ik_+z} + k_- a_3 e^{ik_-z} - k_- a_4 e^{-ik_-z})e^{ik_{0x}x}, \tag{12c}$$

$$H_{1y} = \frac{-i\varepsilon_{zz}}{\gamma k_0 Z_0\big(k_{0x}^2 - \varepsilon_{zz}k_0^2\big)}\Big[\big(k_+^2 + k_{0x}^2 - \varepsilon_{//}k_0^2\big)k_+ \times (a_1 e^{ik_+z} - a_2 e^{-ik_+z}) + \big(k_-^2 + k_{0x}^2 - \varepsilon_{//}k_0^2\big)k_- \times (a_3 e^{ik_-z} - a_4 e^{-ik_-z})\Big]e^{ik_{0x}x}, \tag{12d}$$

$$H_{1z} = \frac{k_{0x}}{Z_0 k_0}E_{1y}, \tag{12e}$$

where $\varepsilon_{//}=\varepsilon_{xx}=\varepsilon_{yy}$. For region 2, the transmitted light exists, and the corresponding magnetic field can be described as

$$\begin{aligned} H_{2x} &= t_3 e^{ik_{0z}(z-d)} e^{ik_{0x}x}, \\ H_{2y} &= t_1 e^{ik_{0z}(z-d)} e^{ik_{0x}x}, \\ H_{2z} &= t_2 e^{ik_{0z}(z-d)} e^{ik_{0x}x}. \end{aligned} \tag{13}$$

By using the Maxwell's equation $\nabla \cdot \vec{H}_2 = 0$, we get the relationship $t_3 = -k_{0z}t_2/k_{0x}$. Meanwhile, by using $\nabla \times \vec{H} = -i\omega\vec{D}$, the components of electric field in region 2 is written as

$$E_{2x} = \frac{Z_0 k_{0z}}{k_0} t_1 e^{ik_{0z}(z-d)} e^{ik_{0x}x}, \tag{14a}$$

$$E_{2y} = \frac{Z_0 k_0}{k_{0x}} t_2 e^{ik_{0z}(z-d)} e^{ik_{0x}x}, \tag{14b}$$

$$E_{2z} = -\frac{Z_0 k_{0x}}{k_0} t_1 e^{ik_{0z}(z-d)} e^{ik_{0x}x}. \tag{14c}$$

Therefore, the components of electric and magnetic fields in regions 0, 1, and 2 are all obtained. Notably, there exist eight parameters, a_1, a_2, a_3, a_4, r_1, r_2, t_1, and t_2, that need to be solved. Fortunately, upon matching the tangential electric and magnetic fields at $z = 0$ and $z = \mathrm{d}$, we can calculate these parameters successfully. For calculating the parameters $(a_1 \quad a_2 \quad a_3 \quad a_4)$, a 4×4 matrix is established as

$$\begin{aligned} &\begin{pmatrix} m_{11} & m_{12} & m_{13} & m_{14} \\ m_{21} & m_{22} & m_{23} & m_{24} \\ m_{31} & m_{32} & m_{33} & m_{34} \\ m_{41} & m_{42} & m_{43} & m_{44} \end{pmatrix} \begin{pmatrix} a_1 \\ a_2 \\ a_3 \\ a_4 \end{pmatrix} \\ &= \begin{pmatrix} 0 \\ -2i\gamma k_0 k_{0z} Z_0 \left(k_{0x}^2 - \varepsilon_{zz} k_0^2\right) \\ 0 \\ 0 \end{pmatrix}, \end{aligned} \tag{15}$$

with the parameters

$$\begin{aligned}
&m_{11} = k_{0z} + k_+, \quad m_{12} = k_{0z} - k_+, \quad m_{13} = k_{0z} + k_-, \quad m_{14} = k_{0z} - k_-, \\
&m_{31} = (k_+ - k_{0z})e^{ik_+ d}, \quad m_{32} = (-k_+ - k_{0z})e^{-ik_+ d}, \quad m_{33} = (k_- - k_{0z})e^{ik_- d}, \quad m_{34} = (-k_- - k_{0z})e^{-ik_- d}, \\
&m_{21} = -\varepsilon_{zz} k_{0z} k_+^3 + \left(k_{0x}^2 - \varepsilon_{zz} k_0^2\right) k_+^2 - \varepsilon_{zz} k_{0z} \left(k_{0x}^2 - \varepsilon_{//} k_0^2\right) k_+ + \left(k_{0x}^2 - \varepsilon_{zz} k_0^2\right)\left(k_{0x}^2 - \varepsilon_{//} k_0^2\right), \\
&m_{22} = \varepsilon_{zz} k_{0z} k_+^3 + \left(k_{0x}^2 - \varepsilon_{zz} k_0^2\right) k_+^2 + \varepsilon_{zz} k_{0z} \left(k_{0x}^2 - \varepsilon_{//} k_0^2\right) k_+ + \left(k_{0x}^2 - \varepsilon_{zz} k_0^2\right)\left(k_{0x}^2 - \varepsilon_{//} k_0^2\right), \\
&m_{23} = -\varepsilon_{zz} k_{0z} k_-^3 + \left(k_{0x}^2 - \varepsilon_{zz} k_0^2\right) k_-^2 - \varepsilon_{zz} k_{0z} \left(k_{0x}^2 - \varepsilon_{//} k_0^2\right) k_- + \left(k_{0x}^2 - \varepsilon_{zz} k_0^2\right)\left(k_{0x}^2 - \varepsilon_{//} k_0^2\right), \\
&m_{24} = \varepsilon_{zz} k_{0z} k_-^3 + \left(k_{0x}^2 - \varepsilon_{zz} k_0^2\right) k_-^2 + \varepsilon_{zz} k_{0z} \left(k_{0x}^2 - \varepsilon_{//} k_0^2\right) k_- + \left(k_{0x}^2 - \varepsilon_{zz} k_0^2\right)\left(k_{0x}^2 - \varepsilon_{//} k_0^2\right), \\
&m_{41} = \left[\varepsilon_{zz} k_{0z} k_+^3 + \left(k_{0x}^2 - \varepsilon_{zz} k_0^2\right) k_+^2 + \varepsilon_{zz} k_{0z} \left(k_{0x}^2 - \varepsilon_{//} k_0^2\right) k_+ + \left(k_{0x}^2 - \varepsilon_{zz} k_0^2\right)\left(k_{0x}^2 - \varepsilon_{//} k_0^2\right)\right] e^{ik_+ d}, \\
&m_{42} = \left[- \varepsilon_{zz} k_{0z} k_+^3 + \left(k_{0x}^2 - \varepsilon_{zz} k_0^2\right) k_+^2 - \varepsilon_{zz} k_{0z} \left(k_{0x}^2 - \varepsilon_{//} k_0^2\right) k_+ + \left(k_{0x}^2 - \varepsilon_{zz} k_0^2\right)\left(k_{0x}^2 - \varepsilon_{//} k_0^2\right)\right] e^{-ik_+ d}, \\
&m_{43} = \left[\varepsilon_{zz} k_{0z} k_-^3 + \left(k_{0x}^2 - \varepsilon_{zz} k_0^2\right) k_-^2 + \varepsilon_{zz} k_{0z} \left(k_{0x}^2 - \varepsilon_{//} k_0^2\right) k_- + \left(k_{0x}^2 - \varepsilon_{zz} k_0^2\right) \times \left(k_{0x}^2 - \varepsilon_{//} k_0^2\right)\right] e^{ik_- d}, \\
&m_{44} = \left[- \varepsilon_{zz} k_{0z} k_-^3 + \left(k_{0x}^2 - \varepsilon_{zz} k_0^2\right) k_-^2 - \varepsilon_{zz} k_{0z} \left(k_{0x}^2 - \varepsilon_{//} k_0^2\right) k_- + \left(k_{0x}^2 - \varepsilon_{zz} k_0^2\right)\left(k_{0x}^2 - \varepsilon_{//} k_0^2\right)\right] e^{-ik_- d}.
\end{aligned}$$

After calculating the parameters $(a_1 \quad a_2 \quad a_3 \quad a_4)$, the other four parameters can be obtained as

$$r_1 = 1 - \frac{i}{\gamma k_0 k_{0z} Z_0} \begin{pmatrix} k_+^2 + k_{0x}^2 - \varepsilon_{//} k_0^2 & k_+^2 + k_{0x}^2 - \varepsilon_{//} k_0^2 & k_-^2 + k_{0x}^2 - \varepsilon_{//} k_0^2 & k_-^2 + k_{0x}^2 - \varepsilon_{//} k_0^2 \end{pmatrix} \begin{pmatrix} a_1 \\ a_2 \\ a_3 \\ a_4 \end{pmatrix}, \tag{16}$$

$$r_2 = \frac{k_{0x}}{k_0 Z_0} \begin{pmatrix} 1 & 1 & 1 & 1 \end{pmatrix} \begin{pmatrix} a_1 \\ a_2 \\ a_3 \\ a_4 \end{pmatrix}, \tag{17}$$

$$t_2 = -\frac{k_{0x}}{k_{0z} k_0 Z_0} \begin{pmatrix} -k_+ e^{ik_+ d} & k_+ e^{-ik_+ d} & -k_- e^{ik_- d} & k_- e^{-ik_- d} \end{pmatrix} \begin{pmatrix} a_1 \\ a_2 \\ a_3 \\ a_4 \end{pmatrix}, \tag{18}$$

$$t_1 = \frac{-i\varepsilon_{zz}}{\gamma k_0 Z_0\left(k_{0x}^2 - \varepsilon_{zz}k_0^2\right)} C \begin{pmatrix} a_1 \\ a_2 \\ a_3 \\ a_4 \end{pmatrix}, \tag{19}$$

$$C = \left[\left(k_+^2 + k_{0x}^2 - \varepsilon_{//}k_0^2\right)k_+ e^{ik_+ d} \quad -\left(k_+^2 + k_{0x}^2 - \varepsilon_{//}k_0^2\right)k_+ e^{-ik_+ d} \quad \left(k_-^2 + k_{0x}^2 - \varepsilon_{//}k_0^2\right)k_- e^{ik_- d} \quad -\left(k_-^2 + k_{0x}^2 - \varepsilon_{//}k_0^2\right)k_- e^{-ik_- d}\right]. \tag{20}$$

Finally, we can obtain the reflection coefficients r_{pp} and r_{ps}, written as

$$r_{pp} = \frac{E_r^p}{E_i^p} = \sqrt{\left[\frac{k_{0z}}{k_0}(1 - r_1) - \cos\theta\right]^2 + \left[-\frac{k_{0x}}{k_0}(1 + r_1) + \sin\theta\right]^2}, \tag{21}$$

$$r_{ps} = \frac{E_r^s}{E_i^p} = \frac{k_0}{k_{0x}} r_2. \tag{22}$$

Similarly, the reflection coefficients r_{ss} and r_{sp}, described as

$$r_{ss} = \frac{E_r^s}{E_i^s} = (1 \quad 1 \quad 1 \quad 1) \begin{pmatrix} a_{1s} \\ a_{2s} \\ a_{3s} \\ a_{4s} \end{pmatrix} - 1, \tag{23}$$

$$r_{sp} = \frac{E_r^p}{E_i^s} = \frac{k_0}{k_{0z}} \frac{i}{\gamma k_0^2} \left(k_+^2 + k_{0x}^2 - \varepsilon_{//}k_0^2 \quad k_+^2 + k_{0x}^2 - \varepsilon_{//}k_0^2 \quad k_-^2 + k_{0x}^2 - \varepsilon_{//}k_0^2 \quad k_-^2 + k_{0x}^2 - \varepsilon_{//}k_0^2\right) \begin{pmatrix} a_{1s} \\ a_{2s} \\ a_{3s} \\ a_{4s} \end{pmatrix}, \tag{24}$$

where the parameters $(a_{1s} \quad a_{2s} \quad a_{3s} \quad a_{4s})$ can be calculated by using the follow matrix equation:

$$\begin{pmatrix} M_{11} & M_{12} & M_{13} & M_{14} \\ M_{21} & M_{22} & M_{23} & M_{24} \\ M_{31} & M_{32} & M_{33} & M_{34} \\ M_{41} & M_{42} & M_{43} & M_{44} \end{pmatrix} \begin{pmatrix} a_{1s} \\ a_{2s} \\ a_{3s} \\ a_{4s} \end{pmatrix} = \begin{pmatrix} 2k_{0z} \\ 0 \\ 0 \\ 0 \end{pmatrix}; \tag{25}$$

here, the relevant parameters are

$$M_{11} = k_{0z} + k_+,$$
$$M_{12} = k_{0z} - k_+,$$
$$M_{13} = k_{0z} + k_-,$$
$$M_{14} = k_{0z} - k_-,$$
$$M_{31} = (k_+ - k_{0z})e^{ik_+ d},$$
$$M_{32} = (-k_+ - k_{0z})e^{-ik_+ d},$$
$$M_{33} = (k_- - k_{0z})e^{ik_- d}, \quad M_{34} = (-k_- - k_{0z})e^{-ik_- d},$$
$$M_{21} = \varepsilon_{zz}k_{0z}k_+^3 - \left(k_{0x}^2 - \varepsilon_{zz}k_0^2\right)k_+^2 + \varepsilon_{zz}k_{0z}\left(k_{0x}^2 - \varepsilon_{//}k_0^2\right)k_+ - \left(k_{0x}^2 - \varepsilon_{zz}k_0^2\right) \times \left(k_{0x}^2 - \varepsilon_{//}k_0^2\right),$$
$$M_{22} = -\varepsilon_{zz}k_{0z}k_+^3 - \left(k_{0x}^2 - \varepsilon_{zz}k_0^2\right)k_+^2 - \varepsilon_{zz}k_{0z}\left(k_{0x}^2 - \varepsilon_{//}k_0^2\right)k_+ - \left(k_{0x}^2 - \varepsilon_{zz}k_0^2\right)\left(k_{0x}^2 - \varepsilon_{//}k_0^2\right),$$
$$M_{23} = \varepsilon_{zz}k_{0z}k_-^3 - \left(k_{0x}^2 - \varepsilon_{zz}k_0^2\right)k_-^2 + \varepsilon_{zz}k_{0z}\left(k_{0x}^2 - \varepsilon_{//}k_0^2\right)k_- - \left(k_{0x}^2 - \varepsilon_{zz}k_0^2\right)\left(k_{0x}^2 - \varepsilon_{//}k_0^2\right),$$
$$M_{24} = -\varepsilon_{zz}k_{0z}k_-^3 - \left(k_{0x}^2 - \varepsilon_{zz}k_0^2\right)k_-^2 - \varepsilon_{zz}k_{0z}\left(k_{0x}^2 - \varepsilon_{//}k_0^2\right)k_- - \left(k_{0x}^2 - \varepsilon_{zz}k_0^2\right)\left(k_{0x}^2 - \varepsilon_{//}k_0^2\right),$$
$$M_{41} = \left[\varepsilon_{zz}k_{0z}k_+^3 + \left(k_{0x}^2 - \varepsilon_{zz}k_0^2\right)k_+^2 + \varepsilon_{zz}k_{0z}\left(k_{0x}^2 - \varepsilon_{//}k_0^2\right)k_+ + \left(k_{0x}^2 - \varepsilon_{zz}k_0^2\right)\left(k_{0x}^2 - \varepsilon_{//}k_0^2\right)\right]e^{ik_+ d},$$
$$M_{42} = \left[-\varepsilon_{zz}k_{0z}k_+^3 + \left(k_{0x}^2 - \varepsilon_{zz}k_0^2\right)k_+^2 - \varepsilon_{zz}k_{0z}\left(k_{0x}^2 - \varepsilon_{//}k_0^2\right)k_+ + \left(k_{0x}^2 - \varepsilon_{zz}k_0^2\right)\left(k_{0x}^2 - \varepsilon_{//}k_0^2\right)\right]e^{-ik_+ d},$$
$$M_{43} = \left[\varepsilon_{zz}k_{0z}k_-^3 + \left(k_{0x}^2 - \varepsilon_{zz}k_0^2\right)k_-^2 + \varepsilon_{zz}k_{0z}\left(k_{0x}^2 - \varepsilon_{//}k_0^2\right)k_- + \left(k_{0x}^2 - \varepsilon_{zz}k_0^2\right)\left(k_{0x}^2 - \varepsilon_{//}k_0^2\right)\right]e^{ik_- d},$$
$$M_{44} = \left[-\varepsilon_{zz}k_{0z}k_-^3 + \left(k_{0x}^2 - \varepsilon_{zz}k_0^2\right)k_-^2 - \varepsilon_{zz}k_{0z}\left(k_{0x}^2 - \varepsilon_{//}k_0^2\right)k_- + \left(k_{0x}^2 - \varepsilon_{zz}k_0^2\right)\left(k_{0x}^2 - \varepsilon_{//}k_0^2\right)\right]e^{-ik_- d}.$$

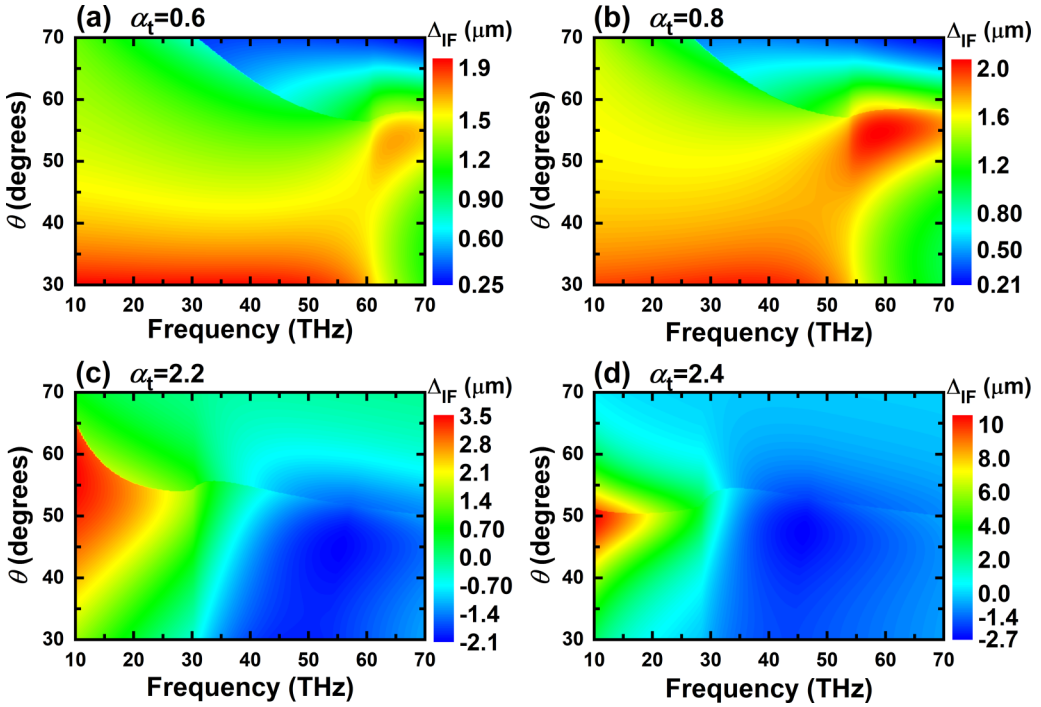

FIG. 2. Pseudocolor images of spatial IF shift as functions of incident angle and frequency. Panels (a) and (b) indicate the spatial IF shift at discrete tilt degrees of 0.6 and 0.8 in type-I WSMs. Panels (c) and (d) exhibit the spatial IF shift at discrete tilt degrees of 2.2 and 2.4 in type-II WSMS, where the Weyl node separation is set as 0.2 nm^{-1}, and the Fermi energy is chosen as 0.2 eV.

Considering a TM-polarized wave illuminating the surface of WSM, the spatial IF shift Δ_{IF}^{H} is written as [40]

$$\Delta_{IF}^{H} = \frac{-R_{sp}\cot\theta[R_{pp}\sin(\phi_{sp}-\phi_{pp})+R_{ss}\sin(\phi_{sp}-\phi_{ss})]}{k_0\left(R_{sp}^2+R_{pp}^2\right)}, \tag{26}$$

where $r_A = R_A\exp(i\phi_A), A = \{pp, ss, sp, ps\}$.

III. DISCUSSIONS AND RESULTS

Notably, the tilt degree and Weyl node separation are two unique and extremely important parameters for determining the optical properties of a WSM. Methods for effectively obtaining these two parameters have therefore become great significance to recognize the optical characteristics of WSM. Generally, precision metrology acts as an important aspect of application of IF shifts. Therefore, studies of IF shift on the surface of a bulk WSM enable the possibility to accurately calculate the tilt degree and Weyl node separation.

A. Determination of tilt degree

The tilt degree of a WSM is an important parameter that can determine the characters of a WSM, and it is often difficult to measure the value of tilt degree. Fortunately, we can realize an accurate calculation of tilt degree by using the phenomenon of spatial IF shift changing from positive to negative near the Brewster angle. For a light with frequency of f illuminating the surface of a bulk WSM, the pseudocolor images of spatial IF shift for a TM wave as functions of incident angle and frequency are shown in Fig. 2. Figures 2(a)–2(d) exhibit the spatial IF shift at different tilt degrees of 0.6, 0.8, 2.2, and 2.4. It can be seen that the spatial IF shifts are always positive for tilt degrees of 0.6 and 0.8 in type-I WSMs. But for tilt degrees of 2.2 and 2.4 in type-II WSMs, the spatial IF shifts change its sign from positive to negative in a small region of incident angle of 50°. Generally, the situation that the spatial IF shifts vary from a positive maximum value to a negative minimum value is mainly caused by Brewster response [34,36,39], and the relevant special angle is called the Brewster angle. Notably, by changing the tilt degree from 2.2 to 2.4, the frequency corresponding to the Brewster effect changes from 35 to 32.9 THz.

For further illustrate the special phenomenon of spatial IF shift, we plot the determination of Brewster angle in Fig. 3. Figures 3(a) and 3(b) exhibit the amplitude of $|r_{pp}|$ and $|r_{sp}|$ as a function of incident angle at a frequency of 35 THz for a tilt degree of 2.2, and at a frequency of 32.9 THz for a tilt degree of 2.4. Obviously, $|r_{pp}|$ varies with the change of incident angle, and we obtain the minimum value, nearly equal to zero, at the incident angle of 50° for these two different cases. This situation means that the Brewster effect has occurred, and the corresponding Brewster angle is 50°. Figures 3(c) and 3(d) denote the spatial IF shift as a function of frequency, where the tilt degrees are 2.2 and 2.4, and the incident angle is chosen as 50° for both cases. It is seen that the spatial IF shift changes from positive to negative at a frequency of 35 THz for a tilt degree of 2.2, and at a frequency of 32.9 THz for a tilt degree of 2.4, which is in good agreement with the results in Figs. 2(c) and 2(d). Therefore, we have proved that the situation of spatial IF shifts varying from a positive maximum value to a negative minimum value is exactly caused by the Brewster angle.

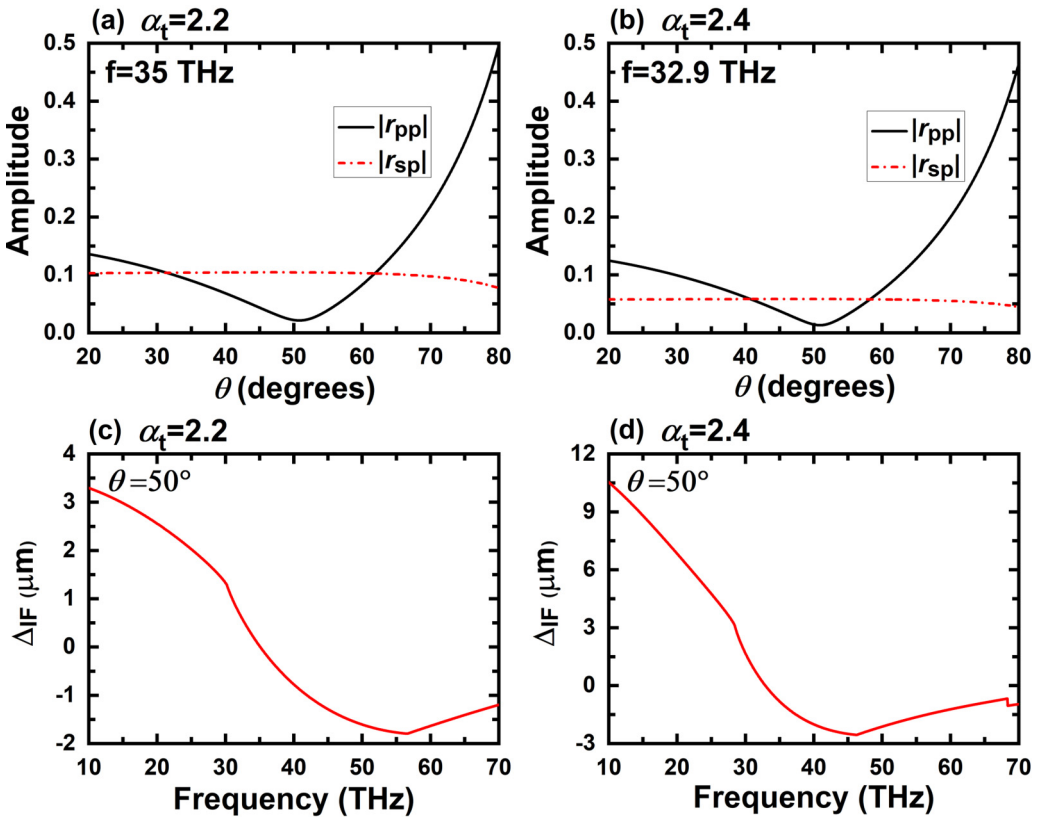

FIG. 3. The determination of Brewster angle. Panels (a) and (b) show the amplitude of $|r_{pp}|$ and $|r_{sp}|$ as a function of incident angle at tilt degrees of 2.2 and 2.4. Panels (c) and (d) exhibit the spatial IF shift as a function of frequency at tilt degrees of 2.2 and 2.4. The frequencies are set as 35 THz in (a) and 32.9 THz in (b), and the incident angles are set as 50° in (c) and (d). Other parameters are identical to those of Fig. 2.

Notably, it is known that the spatial IF shift changes its sign based on the Brewster effect. For a particular tilt degree, this special phenomenon can be realized by simply tuning the frequency at the incident angle near the Brewster angle. Figure 4 exhibits the spatial IF shift as a function of frequency at different tilt degrees when the incident angle is 47° near the Brewster angle. It is obvious that the phenomena of spatial IF shift changing from positive to negative always exist at different tilt degrees. But their respective frequencies are different for different tilt degrees. For instance, the spatial IF shift changes from positive to negative at a frequency of 34.53 THz for a tilt degree of 2.0, at a frequency of 33.81 THz for a tilt degree of 2.2, and at fa requency of 32 THz for a tilt degree of 2.4. With the increase of tilt degree, the respective frequency reduces. Therefore, these tunable phenomena of spatial IF shift changing from positive to negative with a one-to-one correspondence between the tilt degree and frequency enable the feasibility of accurate calculation of tilt degree.

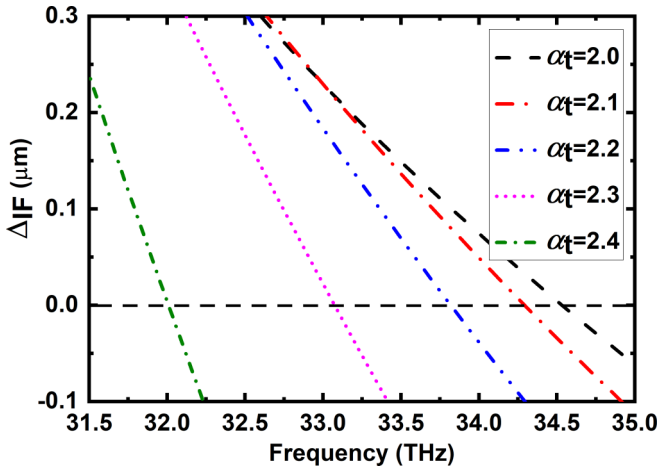

FIG. 4. The phenomenon of spatial IF shift changing from positive to negative by altering the tilt degree and frequency at incident angle of 47°. Other parameters are identical to those of Fig. 2.

B. Determination of Weyl node separation

Besides the tilt degree, the Weyl node separation Q is the other important parameter that determines the anomalous Hall conductivity of a WSM. Here we also can calculate the Weyl node separation Q by using the phenomenon of spatial IF shift changing from positive to negative near the Brewster angle. Figure 5 exhibits the phenomenon of spatial IF shift changing from positive to negative at two different Weyl node separations, where the tilt degree is set as 2.2. The pseudocolor images of spatial IF shift as functions of incident angle and frequency at two different Weyl node separations of 0.18 and 0.21 nm^{-1} are plotted in Figs. 5(a) and 5(b). It is seen that the spatial IF shift change from positive to negative at a frequency of 35.6 THz for a Weyl node separation of 0.18 nm^{-1}, and at a frequency of 34.7 THz for a Weyl node separation of

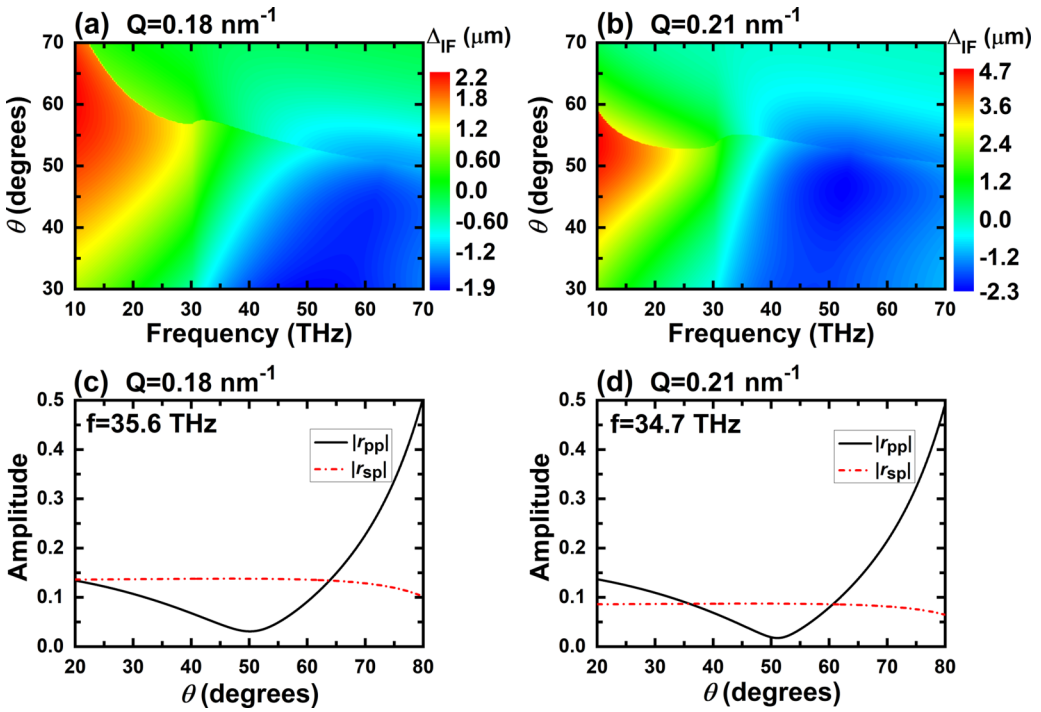

FIG. 5. The phenomenon of spatial IF shift changing from positive to negative at two different Weyl node separations. Panels (a) and (b) show the pseudocolor images of spatial IF shift as functions of incident angle and frequency at different Weyl node separations of 0.18 and 0.21 nm^{-1}. Panels (c) and (d) exhibit the amplitude of $|r_{pp}|$ and $|r_{sp}|$ as a function of incident angle at different Weyl node separations of 0.18 and 0.21 nm^{-1}. The frequencies are set as 35.6 THz in (c) and 34.7 THz in (d), and the Fermi energy is fixed as 0.2 eV.

0.21 nm^{-1}. Meanwhile, both of the spatial IF shifts vary from a positive maximum value to a negative minimum value at an incident angle of 50°, which is caused by the Brewster response. To further determine the Brewster angle, we plot the amplitude of $|r_{pp}|$ and $|r_{sp}|$ as a function of incident angle at a frequency of 35.6 THz for Weyl node separation of 0.18 nm^{-1}, and at a Fermi energy of 34.7 THz for a Weyl node separation of 0.21 nm^{-1}, as shown in Figs. 5(c) and 5(d). Obviously, $|r_{pp}|$ varies with the change of incident angle, and we obtain the minimum value, nearly equal to zero, at the incident angle of 50° for the two different cases. Therefore, we have proved that the situation of spatial IF shifts varying from a positive maximum value to a negative minimum value is exactly caused by a Brewster angle of 50°.

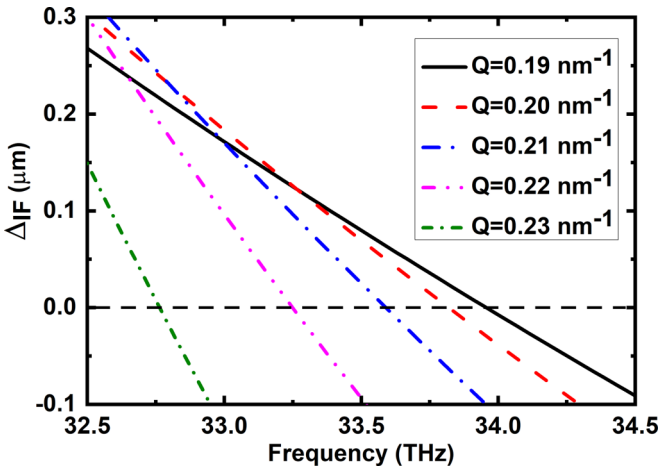

FIG. 6. The phenomenon of spatial IF shift changing from positive to negative by altering the Weyl node separation and frequency at incident angle of 47°.

Notably, based on the above discussion, it is known that when the incident angle is near the Brewster angle, the phenomenon of spatial IF shift changing from positive to negative can be realized at two different Weyl node separations, and its relevant frequency behaves different value. Figure 6 plots the spatial IF shift as a function of frequency at different Weyl node separations, where the incident angle is also chosen as 47°. It is seen that for different Weyl node separations, frequencies corresponding to the spatial IF shift changing from positive to negative are different. For instance, the special phenomenon occurs at a frequency of 33.97 THz for a Weyl node separation of 0.19 nm^{-1}, at a frequency of 33.59 THz for a Weyl node separation of 0.21 nm^{-1}, and at a frequency of 32.77 THz for a Weyl node separation of 0.23 nm^{-1}. With the increase of Weyl node separation, the respective frequency reduces. These tunable phenomena of spatial IF shift changing from positive to negative with one-to-one correspondence between the Weyl node separation and frequency also enable the feasibility of an accurate calculation of Weyl node separation.

IV. CONCLUSIONS

In conclusion, we theoretically study the spatial IF shift at the contact surface of air and bulk WSM. For obtaining the calculation of spatial IF shift, we set up a 4 × 4 magneto-optic

matrix to solve the reflection coefficients by using Maxwell's equations and boundary conditions. It is found that the spatial IF shift changes from a positive value to negative value at the incident angle near 50°. It is further demonstrated that this special phenomenon is caused by the Brewster effect. Interestingly, the phenomenon of spatial IF shift changing from positive to negative can be controlled by changing the frequency of incident light, tilt degree, and Weyl node separation. Specially, for a fixed Weyl node separation, these special phenomena can be realized at different tilt degrees by simply changing the frequency, and there exists a one-to-one correspondence between the tilt degree and frequency at these situations. Therefore, we can determine the tilt degree based on the zero spatial IF shift by shifting the frequency. Similarly, for a fixed tilt degree, these special phenomena of spatial IF shift changing from positive to negative with a one-to-one correspondence between the Weyl node separation and frequency enable the feasibility of an accurate calculation of Weyl node separation. We firmly believe our study is of great significance to recognize the characteristics of a WSM.

ACKNOWLEDGMENTS

This research was supported by the National Natural Science Foundation of China (Grants No. 61875133 and No. 11874269), the Natural Science Foundation of Hunan Province (Grants No. 2021JJ30149, No. 2021JJ30135, and No. 2020JJ5135), the Education Department of Hunan Province (Grants No. 20C0602 and No. 20C0603), and the Science and Technology Project of Shenzhen (Grants No. JCYJ20190808143801672, No. JCYJ20190808150803580, and No. JCYJ20180508152903208).

APPENDIX: CONDUCTIVITIES IN TYPE-I AND TYPE-II WSMs

By introducing the Kubo formula and the real Kramers-Kronig relation, the conductivities of WSMs in type I and type II can be obtained in the low temperature limit ($T = 0\,\mathrm{K}$) [25,41]. Notably, in the case of type-I WSMs with $|\alpha_t| < 1$, the real and imaginary parts of the conductivities are expressed as [25]

$$\mathrm{Re}(\sigma_{xx}) = \begin{cases} 0, & \omega < \omega_l \\ \sigma_\omega(1/2 - \eta_1), & \omega_l < \omega < \omega_u, \\ \sigma_\omega, & \omega > \omega_u \end{cases} \tag{A1}$$

$$\mathrm{Im}(\sigma_{xx}) = -\frac{\sigma_\omega}{4\pi}\left\{\tau(\alpha_t)\ln\left[\frac{|\omega_u^2-\omega^2|}{|\omega_l^2-\omega^2|}\right] + \frac{8}{\alpha_t^2}\left(\frac{\mu}{\hbar\omega}\right)^2 - \left(\frac{\mu}{\hbar\omega}\right)^3 \prod(\omega,\alpha_t,\mu)\ln\left[\frac{|\omega_u-\omega|(\omega_l+\omega)}{|\omega_l-\omega|(\omega_u+\omega)}\right] + \frac{6}{|\alpha_t|^3}\left(\frac{\mu}{\hbar\omega}\right)^2 \ln\left[\frac{|\omega_u^2-\omega^2|\omega_l^2}{|\omega_l^2-\omega^2|\omega_u^2}\right] + 4\ln\left[\frac{|\omega_c^2-\omega^2|}{|\omega_u^2-\omega^2|}\right]\right\}, \tag{A2}$$

$$\mathrm{Re}(\sigma_{zz}) = \begin{cases} 0, & \omega < \omega_l \\ \sigma_\omega\eta_4, & \omega_l < \omega < \omega_u, \\ \sigma_\omega, & \omega > \omega_u \end{cases} \tag{A3}$$

$$\mathrm{Im}(\sigma_{zz}) = -\frac{\sigma_\omega}{2\pi}\left\{\tau'(\alpha_t)\ln\left[\frac{|\omega_u^2-\omega^2|}{|\omega_l^2-\omega^2|}\right] - \frac{8}{\alpha_t^2}\left(\frac{\mu}{\hbar\omega}\right)^2 + \left(\frac{\mu}{\hbar\omega}\right)^3 \prod{}'(\omega,\alpha_t,\mu)\ln\left[\frac{|\omega_u-\omega|(\omega_l+\omega)}{|\omega_l-\omega|(\omega_u+\omega)}\right] - \frac{6}{|\alpha_t|^3}\left(\frac{\mu}{\hbar\omega}\right)^2 \ln\left[\frac{|\omega_u^2-\omega^2|\omega_l^2}{|\omega_l^2-\omega^2|\omega_u^2}\right] + 2\ln\left[\frac{|\omega_c^2-\omega^2|}{|\omega_u^2-\omega^2|}\right]\right\}, \tag{A4}$$

$$\mathrm{Re}(\sigma_{xy}) = \sigma_{xy}^{\mathrm{anom-I}} + \mathrm{sgn}(\alpha_t)\sigma_\mu\left\{\frac{-1}{2\alpha_t^2}\ln\left[\frac{|\omega_u^2-\omega^2|\omega_l^2}{|\omega_l^2-\omega^2|\omega_u^2}\right] + \left(\frac{\mu}{2\hbar\omega\alpha_t^2} + \frac{\hbar\omega}{8\mu}\frac{1-\alpha_t^2}{\alpha_t^2}\right)\ln\left[\frac{|\omega_u-\omega|(\omega_l+\omega)}{|\omega_l-\omega|(\omega_u+\omega)}\right] - \frac{1}{|\alpha_t|}\right\}, \tag{A5}$$

$$\mathrm{Im}(\sigma_{xy}) = \mathrm{sgn}(\alpha_t)\begin{cases} 0, & \omega < \omega_l \\ 3\sigma_\omega\eta_3, & \omega_l < \omega < \omega_u. \\ 0, & \omega > \omega_u \end{cases} \tag{A6}$$

Here, $\sigma_\omega = e^2\omega/(6h\nu_F)$, where e and h represent the elementary charge and the Planck constant, respectively; $\hbar = h/(2\pi)$ is the reduced Planck constant, μ is the Fermi energy; ω is the frequency of light; $\nu_F = 10^6\mathrm{m/s}$ denotes the Fermi velocity; $\omega_c = k_c\nu_F$ is the ultraviolet cutoff frequency, in which k_c denotes the momentum cutoff along the k_z axis; $\omega_l = 2\mu/[\hbar(1+|\alpha_t|)]$, $\omega_u = 2\mu/[\hbar(1-|\alpha_t|)]$, $\tau(\alpha_t) = 2 + 1/(2|\alpha_t|^3) + 3/(2|\alpha_t|)$, $\tau'(\alpha_t) = 1 - 1/(2|\alpha_t|^3) + 3/(2|\alpha_t|)$ $\sigma_\mu = e^2\mu/(h^2\nu_F)$; and the other related parameters are written as follows:

$$\eta_1 = \frac{3}{8|\alpha_t|}\left(\frac{2\mu}{\hbar\omega} - 1\right)\left[1 + \frac{1}{3\alpha_t^2}\left(\frac{2\mu}{\hbar\omega} - 1\right)^2\right], \tag{A7}$$

$$\eta_3 = \frac{1}{\alpha_t^2}\left(\frac{1}{8} - \frac{\mu}{2\hbar\omega} + \frac{\mu^2}{2\hbar^2\omega^2}\right) - \frac{1}{8}, \tag{A8}$$

$$\eta_4 = \frac{1}{2} + \frac{(2\mu - \hbar\omega)^3}{4\hbar^3\omega^3|\alpha_t|^3} + \frac{1}{|\alpha_t|}\left(\frac{3}{4} - \frac{3\mu}{2\hbar\omega}\right), \tag{A9}$$

$$\prod(\omega, \alpha_t, \mu) = \frac{4}{|\alpha_t|^3} + 3\left(\frac{\hbar\omega}{\mu}\right)^2\left(\frac{1}{|\alpha_t|^3} + \frac{1}{|\alpha_t|}\right), \tag{A10}$$

$$\prod'(\omega, \alpha_t, \mu) = \frac{4}{|\alpha_t|^3} + 3\left(\frac{\hbar\omega}{\mu}\right)^2\left(\frac{1}{|\alpha_t|^3} - \frac{1}{|\alpha_t|}\right), \tag{A11}$$

$$\sigma_{xy}^{\text{anom-I}} = \sigma_Q + \sigma_\mu\left[\frac{2}{\alpha_t} + \frac{1}{\alpha_t^2}\ln\left(\frac{1-\alpha_t}{1+\alpha_t}\right)\right], \tag{A12}$$

where $\sigma_Q = e^2Q/(\pi h)$, which is a function of Q.

Meanwhile, in the case of type-II WSMs with $|\alpha_t| > 1$, the real and imaginary parts of the conductivities are described as [25]

$$\mathrm{Re}(\sigma_{xx}) = \begin{cases} 0, & \omega < \omega_l \\ \sigma_\omega(1/2 - \eta_1), & \omega_l < \omega < \omega'_u, \\ \sigma_\omega\eta_2, & \omega > \omega'_u \end{cases} \tag{A13}$$

$$\begin{aligned}\mathrm{Im}(\sigma_{xx}) = -\frac{\sigma_\omega}{4\pi}\Bigg\{&\tau(\alpha_t)\ln\left[\frac{\left|{\omega'_u}^2 - \omega^2\right|}{\left|\omega_l^2 - \omega^2\right|}\right] + \frac{8}{\alpha_t^3}\left(\frac{\mu}{\hbar\omega}\right)^2 - \left(\frac{\mu}{\hbar\omega}\right)^3\prod(\omega, \alpha_t, \mu)\ln\left[\frac{|\omega'_u - \omega|(\omega_l + \omega)}{|\omega_l - \omega|(\omega'_u + \omega)}\right] \\ &+ \frac{6}{|\alpha_t|^3}\left(\frac{\mu}{\hbar\omega}\right)^2\ln\left[\frac{\left|{\omega'_u}^2 - \omega^2\right|\omega_l^2}{\left|\omega_l^2 - \omega^2\right|{\omega'_u}^2}\right] + \left(\frac{3}{|\alpha_t|} + \frac{1}{|\alpha_t|^3}\right)\ln\left[\frac{\left|\omega_c^2 - \omega^2\right|}{\left|{\omega'_u}^2 - \omega^2\right|}\right] + \frac{12}{|\alpha_t|^3}\left(\frac{\mu}{\hbar\omega}\right)^2\ln\left[\frac{\left|\omega_c^2 - \omega^2\right|{\omega'_u}^2}{\left|{\omega'_u}^2 - \omega^2\right|\omega_c^2}\right]\Bigg\},\end{aligned} \tag{A14}$$

$$\mathrm{Re}(\sigma_{zz}) = \begin{cases} 0, & \omega < \omega_l \\ \sigma_\omega\eta_4, & \omega_l < \omega < \omega'_u, \\ \sigma_\omega\eta_5, & \omega > \omega'_u \end{cases} \tag{A15}$$

$$\begin{aligned}\mathrm{Im}(\sigma_{zz}) = -\frac{\sigma_\omega}{2\pi}\Bigg\{&\tau'(\alpha_t)\ln\left[\frac{\left|{\omega'_u}^2 - \omega^2\right|}{\left|\omega_l^2 - \omega^2\right|}\right] - \frac{8}{\alpha_t^3}\left(\frac{\mu}{\hbar\omega}\right)^2 + \left(\frac{\mu}{\hbar\omega}\right)^3\prod'(\omega, \alpha_t, \mu)\ln\left[\frac{|\omega'_u - \omega|(\omega_l + \omega)}{|\omega_l - \omega|(\omega'_u + \omega)}\right] \\ &- \frac{6}{|\alpha_t|^3}\left(\frac{\mu}{\hbar\omega}\right)^2\ln\left[\frac{\left|{\omega'_u}^2 - \omega^2\right|\omega_l^2}{\left|\omega_l^2 - \omega^2\right|{\omega'_u}^2}\right] + \left(\frac{3}{\alpha_t} - \frac{1}{{\alpha_t}^3}\right)\ln\left[\frac{\left|\omega_c^2 - \omega^2\right|}{\left|{\omega'_u}^2 - \omega^2\right|}\right] - \frac{12}{|\alpha_t|^3}\left(\frac{\mu}{\hbar\omega}\right)^2\ln\left[\frac{\left|\omega_c^2 - \omega^2\right|{\omega'_u}^2}{\left|{\omega'_u}^2 - \omega^2\right|\omega_c^2}\right]\Bigg\},\end{aligned} \tag{A16}$$

$$\begin{aligned}\mathrm{Re}(\sigma_{xy}) = \sigma_{xy}^{\text{anom}-\text{II}} + \mathrm{sgn}(\alpha_t)\sigma_\mu\Bigg\{&\frac{-1}{2\alpha_t^2}\ln\left[\frac{\left(\omega_c^2 - \omega^2\right)^2\omega_l^2{\omega'_u}^2}{\left|\omega_l^2 - \omega^2\right|\left|{\omega'_u}^2 - \omega^2\right|\omega_c^4}\right] \\ &+ \left(\frac{\mu}{2\hbar\omega\alpha_t^2} + \frac{\hbar\omega}{8\mu}\frac{1-\alpha_t^2}{\alpha_t^2}\right)\ln\left[\frac{|\omega'_u - \omega|(\omega_l + \omega)}{|\omega_l - \omega|(\omega'_u + \omega)}\right] - \frac{2}{\alpha_t^2}\Bigg\},\end{aligned} \tag{A17}$$

$$\mathrm{Im}(\sigma_{xy}) = \mathrm{sgn}(\alpha_t)\begin{cases} 0, & \omega < \omega_l \\ 3\sigma_\omega\eta_3, & \omega_l < \omega < \omega'_u. \\ \frac{-3\mu\sigma_\omega}{\hbar\omega\alpha_t^2}, & \omega > \omega'_u \end{cases} \tag{A18}$$

Here, $\omega'_u = 2\mu/[\hbar(|\alpha_t| - 1)]$; and the other related parameters are written as follows:

$$\eta_2 = \frac{3}{4|\alpha_t|}\left[1 + \frac{1}{3\alpha_t^2} + \left(\frac{2\mu}{\alpha_t\hbar\omega}\right)^2\right], \tag{A19}$$

$$\eta_5 = \frac{-1}{2|\alpha_t|^3}\left[1 - 3{\alpha_t}^2 + \frac{12\mu^2}{\hbar^2\omega^2}\right], \tag{A20}$$

$$\sigma_{xy}^{\text{anom-II}} = \frac{\sigma_Q}{|\alpha_t|} + \frac{\mathrm{sgn}(\alpha_t)\sigma_\mu}{\alpha_t^2}\ln\left[\frac{\mu^2}{\hbar^2\omega_c^2\alpha_t^2\left(\alpha_t^2 - 1\right)}\right]. \tag{A21}$$

[1] A. A. Burkov and L. Balents, Phys. Rev. Lett. **107**, 127205 (2011).

[2] C. K. Chan, P. A. Lee, K. S. Burch, J. H. Han, and Y. Ran, Phys. Rev. Lett. **116**, 026805 (2016).

[3] N. P. Armitage, E. J. Mele, and A. Vishwanath, Rev. Mod. Phys. **90**, 015001 (2018).

[4] E. Hendry, P. J. Hale, J. Moger, A. K. Savchenko, and S. A. Mikhailov, Phys. Rev. Lett. **105**, 097401 (2010).

[5] S. Shareef, Y. S. Ang, and C. Zhang, J. Opt. Soc. Am. B **29**, 274 (2012).

[6] K. J. A. Ooi, Y. S. Ang, Q. Zhai, D. T. H. Tan, L. K. Ang, and C. K. Ong, APL Photon. **4**, 034402 (2019).

[7] L. Ju, B. Geng, J. Horng, C. Girit, M. Martin, Z. Hao, H. A. Bechtel, X. Liang, A. Zettl, Y. R. Shen, and F. Wang, Nat. Nanotechnol. **6**, 630 (2011).

[8] A. A. Zyuzin and A. A. Burkov, Phys. Rev. B **86**, 115133 (2012).

[9] K. Halterman, M. Alidoust, and A. Zyuzin, Phys. Rev. B **98**, 085109 (2018).

[10] E. Liu, Y. Sun, N. Kumar, L. Meuchler, A. Sun, J. Lin, S. Yang, D. Liu, A. Liang, Q. Xu, J. Kroder, V. Seuss, H. Borrmann, C. Shekhar, Z. Wang, C. Xi, W. Wang, W. Schnelle, S. Wirth, Y. Chen, S. T. B. Goennenwein, and C. Felser, Nat. Phys. **14**, 1125 (2018).

[11] S. Xu, B. Ilya, A. Nasser, N. Madhab, G. Bian, C. Zhang, S. Raman, G. Chang, Z. Yuan, C. Lee, S. Huang, H. Zheng, J. Ma, D. S. Sanchez, B. Wang, A. Bansil, F. Chou, P. P. Shibayev, H. Lin, S. Jia, and M. Z. Hasan, Science **349**, 613 (2015).

[12] B. Q. Lv, H. M. Weng, B. B. Fu, X. P. Wang, H. Miao, J. Ma, P. Richard, X. C. Huang, L. X. Zhao, G. F. Chen, Z. Fang, X. Dai, T. Qian, and H. Ding, Phys. Rev. X **5**, 031013 (2015).

[13] S. Huang, S. Xu, I. Belopolski, C. C. Lee, G. Chang, B. K. Wang, N. Alidoust, G. Bian, M. Neupane, and C. Zhang, Nat. Commun. **6**, 7373 (2015).

[14] L. Lu, Z. Wang, D. Ye, L. Ran, L. Fu, J. D. Joannopoulos, and M. Soljacic, Science **349**, 622 (2015).

[15] W. Meng, X. Zhang, T. He, L. Jin, X. Dai, Y. Liu, and G. Liu, J. Adv. Res. **24**, 523 (2020).

[16] A. A. Soluyanov, D. Gresch, Z. Wang, Q. Wu, M. Troyer, X. Dai, and B. A. Bernevig, Nature (London) **527**, 495 (2015).

[17] Y. Wang, E. Liu, H. Liu, Y. Pan, L. Zhang, J. Zeng, Y. Fu, M. Wang, K. Xu, and Z. Huang, Nat. Commun. **7**, 13142 (2016).

[18] K. Deng, G. Wan, P. Deng, K. Zhang, S. Ding, E. Wang, M. Yan, H. Huang, H. Zhang, and Z. Xu, Nat. Phys. **12**, 1105 (2016).

[19] Y. Ferreiros, A. A. Zyuzin, and J. H. Bardarson, Phys. Rev. B **96**, 115202 (2017).

[20] P. Hosur, S. A. Parameswaran, and A. Vishwanath, Phys. Rev. Lett. **108**, 046602 (2012).

[21] S. Wang, B. Lin, A. Wang, D. Yu, and Z. Liao, Adv. Phys.: X **2**, 518 (2017).

[22] K. Das and A. Agarwal, Phys. Rev. B **99**, 085405 (2019).

[23] F. Wilczek, Phys. Rev. Lett. **58**, 1799 (1987).

[24] L. Wu, M. Salehi, N. Koirala, J. Moon, S. Oh, and N. P. Armitage, Science **354**, 1124 (2016).

[25] K. Sonowal, A. Singh, and A. Agarwal, Phys. Rev. B **100**, 085436 (2019).

[26] M. Onoda, S. Murakami, and N. Nagaosa, Phys. Rev. Lett. **93**, 083901 (2004).

[27] K. Y. Bliokh and Y. P. Bliokh, Phys. Rev. Lett. **96**, 073903 (2006).

[28] O. Hosten and P. Kwiat, Science **319**, 787 (2008).

[29] X. Zhou, L. Sheng, and X. Ling, Sci. Rep. **8**, 1221 (2018).

[30] X. Zhou, X. Ling, H. Luo, and S. Wen, Appl. Phys. Lett. **101**, 251602 (2012).

[31] N. Li, T. Tang, J. Li, L. Luo, C. Li, J. Shen, and J. Yao, J. Magn. Magn. Mater. **484**, 445 (2019).

[32] Q. D. Jiang, H. Jiang, H. Liu, Q. Sun, and X. C. Xie, Phys. Rev. Lett. **115**, 156602 (2015).

[33] Q. D. Jiang, H. Jiang, H. Liu, Q. Sun, and X. C. Xie, Phys. Rev. B **93**, 195165 (2016).

[34] S. Chen, C. Mi, W. Wu, W. Zhang, W. Shu, H. Luo, and S. Wen, New J. Phys. **20**, 103050 (2018).

[35] S. Liu, Y. Shou, X. Zhou, W. Cheng, and Z. Luo, Opt. Express **28**, 10783 (2020).

[36] M. Kargarian, M. Randeria, and N. Trivedi, Sci. Rep. **5**, 12683 (2015).

[37] A. G. Grushin, J. W. F. Venderbos, and J. H. Bardarson, Phys. Rev. B **91**, 121109(R) (2015).

[38] P. Rodriguez-Lopez, A. Popescu, I. Fialkovsky, N. Khusnutdinov, and L. M. Woods, Commun. Mater. **1**, 14 (2020).

[39] O. V. Kotov and Y. E. Lozovik, Phys. Rev. B **93**, 235417 (2016).

[40] G. Ye, W. Zhang, W. Wu, S. Chen, W. Shu, H. Luo, and S. Wen, Phys. Rev. A **99**, 023807 (2019).

[41] S. Ahn, E. J. Mele, and H. Min, Phys. Rev. B **95**, 161112(R) (2017).